Renewable Energy 156 (2020) 220–234

Contents lists available at ScienceDirect

Renewable Energy

journal homepage: www.elsevier.com/locate/renene

A general optimal operating strategy for commercial membrane distillation facilities

Juan D. Gil [a], Paulo R.C. Mendes [c, d], E. Camponogara [c], Lidia Roca [a, b], J.D. Álvarez [a, *], Julio E. Normey-Rico [c]

[a] Centro Mixto CIESOL, ceiA3, Universidad de Almería, Ctra, Sacramento s/n, Almería, 04120, Spain
[b] CIEMAT-Plataforma Solar de Almería, Ctra, de Senés s/n, Tabernas, 04200, Almería, Spain
[c] Federal University of Santa Catarina, Department of Automation and Systems engineering, Florianópolis, Brazil
[d] Fraunhofer Institute for Industrial Mathematics, Kaiserslautern, Germany

ARTICLE INFO

Article history:
Received 23 December 2019
Received in revised form
4 March 2020
Accepted 13 April 2020
Available online 23 April 2020

Keywords:
Thermal efficiency
Desalination
Solar energy
Benders decomposition
Model predictive control

ABSTRACT

The high thermal energy consumption is one of the main drawbacks hampering the commercial implementation of Membrane Distillation (MD) technology. The development of adequate operating strategies can help to reduce these energy requirements. Accordingly, this paper focuses on the optimal management of the array of MD modules composing a commercial-scale MD plant, trying to reduce their thermal energy consumption while ensuring a given water need. For this aim, the array of MD modules is modelled as a Mixed Integer Programming (MIP) system to consider that some modules can be turned on/off depending on the operation specifications. An algorithm based on the Generalized Bender Decomposition (GBD) is then developed for the efficient solution of the problem. This algorithm is incorporated in a Model Predictive Control (MPC) strategy allowing to manage the plant in real time. The effectiveness of the proposed strategy is verified using a practical example. The obtained results are compared with a manual and a previous strategy presented in literature, showing that for a sunny day, around the 65 and 55% of the thermal energy consumed by these methodologies can be saved, which means important thermal energy savings that can be relevant for the industrial implementation of MD technology.

1. Introduction

Membrane Distillation (MD) is an arising thermally driven separation method under investigation. This technology enables the use of low-grade thermal energy to desalinate water, what puts MD based processes in a competitive position to relieve water-energy stress nexus sustainably [1]. Despite this fact, its low energy efficiency, mainly caused by its high thermal energy consumption per unit of distillate produced, has hampered the industrial commercialization of the technology so far [2].

From the process point of view, MD stands out from conventional desalination technologies as: i) it is able to treat high salinity feed waters [3], ii) it has a high rejection factor [4], iii) it is driven by the partial pressure difference between both sides of the membrane, which is originated by a temperature difference instead of a mechanical power that increases exergy and costs [5], iv) it operates at low pressure around 0.1 MPa, which is much lower than the one required by Reverse Osmosis (RO) processes 2.5–8.5 MPa [5], and v) it is conducted at low temperature (lower than 90 °C), which allows MD units to be coupled with low grade solar energy [4,6]. This last advantage, together with the simplicity of the process, make MD systems especially suitable for developing stand-alone plants to be applied in offgrids locations; with good irradiance conditions and small-medium water needs [7]. Nevertheless, for making MD technology competitive at industrial-scale, its specific thermal energy consumption must be reduced by improving both the MD module design and configuration [8], and the operating strategies [6].

Regarding the design of MD modules, remarkable improvements have been reported in the literature in the last decades.

* Corresponding author.
E-mail addresses: juandiego.gil@ual.es (J.D. Gil), paulo.mendes@itwm.fraunhofer.de (P.R.C. Mendes), Eduardo.Camponogara@ufsc.br (E. Camponogara), lidia.roca@psa.es (L. Roca), jhervas@ual.es (J.D. Álvarez), julio.normey@ufsc.br (J.E. Normey-Rico).

https://doi.org/10.1016/j.renene.2020.04.074
0960-1481/

These investigations were aimed at creating new membranes, configurations and modules, and to understand the membrane fouling [2]. These research efforts have caused a breakthrough in terms of thermal efficiency, going from a specific thermal energy consumption of 628 kWh/m^3 (MD modules without heat recovery [9]) to the current consumption of commercial-scale modules, around 100 kWh/m^3 at optimal operating conditions [10]. Note that this number is far from the consumption of conventional processes as RO, around 2–4 kWh/m^3 [11]. However, as was pointed out before, what is interesting of MD technology is that these energy requirements (around 95%) can be provided by solar energy [12]. Consequently, there are also numerous works proposing effective combinations [13] and new designs of integrated solar membrane-based desalination systems [14], showing that the overall efficiency can be improved up to 15%. Undoubtedly, the development in the design of the modules is still an open research field, but due to the growth of the technology, other research areas focused on the operation of MD modules are gaining interest in recent years. These works are mainly aimed to optimize the operating parameters of MD units [15], and to develop control and optimal management methods for improving the performance of the technology in real time [7].

With respect to the optimization of the operating parameters, several authors are working on the development of effective statistical or black-box models that allow to find optimal operating conditions of MD units [16]. The statistical model most widely used for this aim is the Response Surface Methodology (RSM). These kind of research works are based on the same procedure [17–20]: i) to design and conduct an experimental campaign in a determined operating range, ii) to adjust the selected outputs of the model by means of the RSM method, and iii) to find the optimal operating conditions within the studied operating range by applying an optimization method. Similarly, other authors used black-box models based on Artificial Neural Networks instead of RSM models with the same objectives [19,21,22]. Even though all these studies show how the thermal efficiency can be considerably improved by using the optimal static operating conditions they present, these conditions are difficult to achieve when using an energy source with an intermittent nature such as solar energy [23].

In this sense, the development of control and optimal operating strategies to be applied in real-time become essential. In Ref. [24] two control modes based on on/off controllers for the day and night were presented in simulation, trying to maintain the distillate production stable even in cloudy days. A neural network based controller that optimizes the distillate production under intermittent conditions was presented and experimentally tested in Ref. [25]. In spite of irradiance disturbances, a feedback control system with reference governor for fixing a suitable operating temperature at the inlet of the MD module was proposed and experimentally tested in Ref. [26]. Moreover, the work [7] experimentally demonstrated that the thermal energy demand of an MD module can be reduced in 1.21 kWh/m^3 by making an optimal management of the solar field powering it. In summary, the works presented above are fundamentally focused on the operation of the solar field, rejecting irradiance disturbances and maintaining desired temperature setpoints to maximize both, distillate production and thermal energy efficiency. However, not only the temperature affects the performance of MD modules but also the feed water flow rate [27]. The optimal management of this variable is especially relevant because a tradeoff solution must be adopted to maximize both thermal efficiency and distillate production in current commercial-scale MD modules [19,28], thus requiring properly formulated optimization problems.

In industrial-scale plants, the optimal operation of the feed water flow rate is even more critical. Due to the low production of current MD commercial modules (around 30 L/h in optimal operating conditions [18]), an industrial-scale plant must include multiple MD units. Accordingly, an optimal management of this variable can considerably reduce the Specific Thermal Energy Consumption (STEC) of the facility. To the best of the authors knowledge, only a previous work [29] deals with this problem. In that work, a distributed Model Predictive Control (MPC) approach was proposed aimed at reducing the STEC while assuring water needs. The tests performed in that work demonstrated how the distributed MPC controller can reduce by 5% the mean STEC of the operation. This percentage means a thermal energy saving of about 50 MWh per season in an application in which an MD industrial plant is combined with an 8 ha cultivation area. Nevertheless, it should be commented that the principal objective of that work was to demonstrate how an effective distributed MPC technique can manage the facility optimally when the water resources were limited and not all the MD modules could be fed at their optimal operating range. In this way, in the formulation of the control system, only continuous variables for the feed water flow rate (within its operating range 400–600 L/h) were considered.

Motivated by the above literature review, the main gaps observed in terms of MD operational strategies are the followings:

1. The real-time management methods proposed in the literature for Solar-powered MD (SMD) systems are focused on the heat generation circuit. The optimal operation of the feed water flow rate of the MD modules has hardly been addressed in these real-time methodologies, which can significantly improve the energy efficiency especially if the water demand is variable.
2. The developed methods are mainly applied to pilot-scale plants. In industrial plants, the presence of multiple MD modules totally alters the formulation of the problem, which has not been well discussed in the aforementioned literature.
3. The only published work that addresses the management of an industrial-scale plant uses only continuous variables in the optimization problem. With this formulation only the STEC can be minimized. If binary variables for turning on and off MD modules are introduced in the problem, the distillate production can be better adapted to the water demand.

In order to address the above issues, in the present work it is proposed a general optimal operating strategy for reducing the total thermal energy consumption of commercial-scale SMD plants connected to a consumer agent. The strategy is focused on the management of the desalination unit of the facility, as the optimal management of the solar field has been previously treated in the literature [7,25,26]. The contributions developed in this paper are the followings: firstly, conventional models used in MD systems are adapted to the Mixed Integer Programming (MIP) methodology. In this formulation, the binary variables are related to valve apertures that allows to turn on/off the MD units installed in the facility, whereas the continuous variables are related to the feed water flow rate of each MD module. Based on this model, a Mixed Integer Nonlinear Programming (MINLP) optimization problem is formulated, tasked with reducing both the STEC and the total thermal energy consumption, while assuring the water requirements. Secondly, it is proposed an efficient algorithm based on the Generalized Benders Decomposition (GBD) method [30] that enables the use of simpler optimization solvers, Mixed Integer Linear Programming (MILP) and Quadratic Programming (QP) methods rather than MINLP for solving the overall problem, which proved to reach optimal results more efficiently. This algorithm is then incorporated into an MPC controller [31] which reflects the operational strategy. Thirdly, to demonstrate the effectiveness of our proposal,

we present an exhaustive analysis by applying the developed technique in a practical case study, and comparing the obtained results to those obtained with a non-optimal management method (a manual operation) and with the ones obtained with the previous approach presented in Ref. [29]. This analysis evidences significant gains in relation to previous/manual approaches showing for example that for a sunny day, around the 65 and 55% of the thermal energy consumed by these operating methodologies can be saved, which can mean important contributions toward the commercialization of MD technology.

The rest of the paper is arranged as follows: Section 2 is dedicated to the description of the system and the optimization problem associated to the management of the facility. Section 3 is aimed at formulating the proposed operating strategy. Section 4 shows the performance of the management technique in a practical case study, and Section 5 summerizes the conclusion obtained from the results.

2. System description and problem formulation

2.1. System description

Fig. 1 shows a general schematic diagram of an SMD plant used for desalination purposes [4]. In this plant, a solar thermal field is used as thermal source. The outlet of the solar field is coupled to a storage tank that is used as buffer system for damping irradiance disturbances or storing the remaining thermal energy of the process. Then, a heat exchanger is employed to connect the MD modules and the heat generation circuit. As can be seen, the desalination unit is formed by an array of MD modules which are bonded in parallel according to Fig. 2. The feed water enters the MD unit, which uses the thermal energy transferred by the solar field to produce distillate and brine. In the process, the brine is rejected while the distillate is stored in the distillate tank. Finally, the water demand agent takes the required freshwater from this tank.

Regarding the operation of the MD modules, as illustrated in Fig. 2, the feed water is pumped by a main pipe to which all the MD modules are joined. The available valves (V_m in Fig. 2) allow to turn on/off each MD module. If a module is in operation, the feed water flows through the condenser channel. In this stage, the feed solution is preheated with the latent heat of condensation and with the sensible heat that crosses the membrane. Afterwards, the preheated solution is circulated to the heat exchanger where it is heated with the fluid coming from the solar field storage tank. Later, the hot solution flows through the evaporator channel where the volatile molecules are evaporated and pass through the membrane and the non-volatile ones are rejected in the form of brine. At the end, the volatile molecules are condensed and driven to the distillate tank. A more complete description of the process can be found elsewhere [10,18].

2.2. MD module modelling

As this work is focused on the management of the desalination unit, a model that accurately represents the behaviour of each of the MD modules contained in the unit must be used for the formulation of the problem. As was mentioned in the introduction section, most works presented in the literature use the RSM methodology as the modelling approach. This method provides linear or quadratic polynomial functions obtained from experimental data to fit the outputs of MD processes. In this work, we use the RSM models presented in Refs. [10,18,29]. By following these works, each subsystem m, i.e. each MD module included in the array, can be modelled according to Fig. 3. So, each subsystem m is characterized by:

- Input: feed water flow rate ($F_m(k) \in \Re_+$).
- Outputs: distillate production ($d_m(k) \in \Re_+$) and the temperature difference ($\Delta T_m(k) \in \Re_+$) between the outlet of the condenser channel ($T_{cout,m}$) and the inlet of the evaporator channel ($T_{ein,m}$) of the MD module. It should be remarked that this variable can be considered as the driving force of the process, which will be used to calculate the amount of thermal energy consumed by each MD module.
- Disturbances: inlet temperature of the condenser channel of the MD module ($T_{cin,m}(k) \in \Re_+$) and inlet temperature of the evaporator channel of the MD module ($T_{ein,m}(k) \in \Re_+$).

where p_i, with $i = 1,\ldots,9$, are constant polynomial coefficients, and the rest of variables are defined in Appendix A.

$$d_m(k) = p_1 + p_2 \cdot T_{ein,m}(k) + p_3 \cdot T_{cin,m}(k) + p_4 \cdot F_m(k) + p_5 \cdot T_{ein,m}(k) \cdot F_m(k), \quad (1)$$

$$\Delta T_m(k) = p_6 + p_7 \cdot T_{ein,m}(k) + p_8 \cdot T_{cin,m}(k) + p_9 \cdot F_m(k), \quad (2)$$

$$d_m(k) = \alpha^d_{m,1}(k) \cdot \delta_m(k) + \alpha^d_{m,2}(k) \cdot F_m(k), \quad (3)$$

$$\Delta T_m(k) = \alpha^T_{m,1}(k) \cdot \delta_m(k) + \alpha^T_{m,2}(k) \cdot F_m(k), \quad (4)$$

where:

$$\alpha^d_{m,1}(k) = p_1 + p_2 \cdot T_{ein,m}(k) + p_3 \cdot T_{cin,m}(k), \quad (5)$$

$$\alpha^d_{m,2}(k) = p_4 + p_5 \cdot T_{ein,m}(k), \quad (6)$$

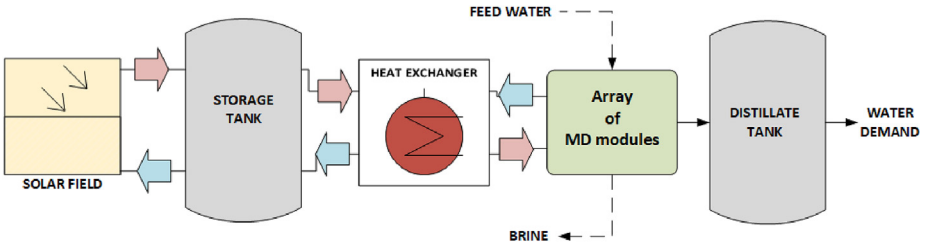

Fig. 1. Schematic diagram of an industrial-scale SMD plant.

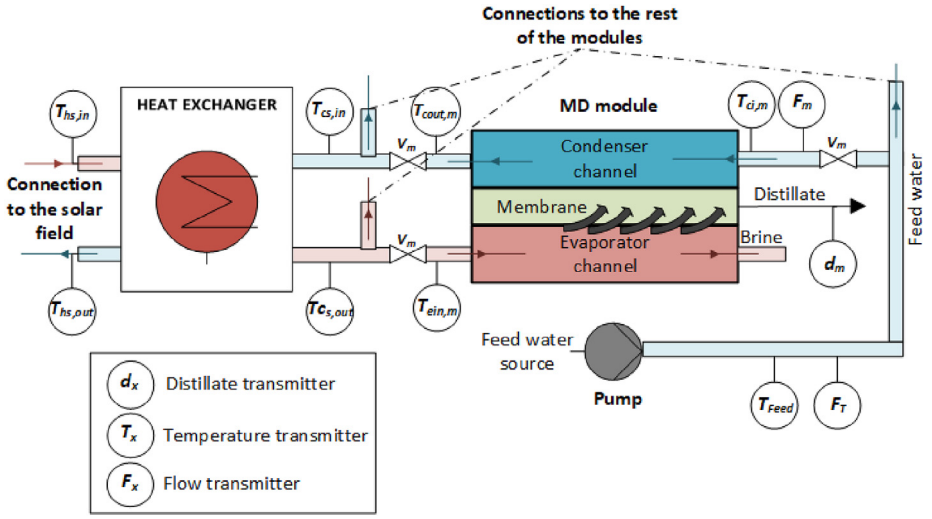

Fig. 2. Connection of a single MD module in the array of MD modules.

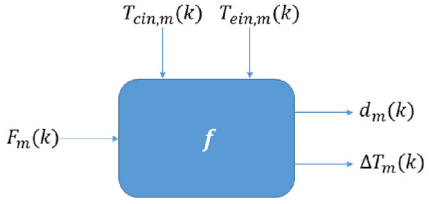

Fig. 3. Single MD module characterization. *f* denotes a linear function.

Note that k is related to the current time. Thus, following the ideas proposed in Refs. [10,18,29], the model of a single MD m-module can be written in a generic way as.

2.3. MIP modelling of the array of MD modules

To formulate the whole optimization problem, binary variables have been introduced in the model presented above. These variables are physically related to the valves located at the inputs and outputs of each MD module (V_m in Fig. 2). In this way, considering $\mathscr{M} = \{1, \ldots, m\}$ the set of MD modules in the array, the MIP model of the whole system can be written as, $\forall m \in \mathscr{M}$:

$$\alpha^T_{m,1}(k) = p_6 + p_7 \cdot T_{ein,m}(k) + p_8 \cdot T_{cin,m}(k), \tag{7}$$

$$\alpha^T_{m,2}(k) = p_9, \tag{8}$$

$$\delta_m(k) \in \{0, 1\}, \tag{9}$$

$$\delta_m(k) \cdot F_m^{Min} \leq F_m(k) \leq \delta_m(k) \cdot F_m^{Max}, \tag{10}$$

F_m^{Min} and F_m^{Max} are the minimum and maximum feed flow rate allowed of each MD module respectively, and δ_m denotes the binary variable related to the valve of MD m-module, which assumes value 1 if the valve is open and 0 otherwise.

In addition, it must be remarked that all the subsystems are coupled by the total distillate production, $d_T(k)$, and by the total water flow rate income $F_T(k)$, which is:

$$\sum_{m \in \mathscr{M}} d_m(k) = d_T(k), \tag{11}$$

$$\sum_{m \in \mathscr{M}} F_m(k) = F_T(k), \tag{12}$$

$$F_T^{Min} \leq F_T(k) \leq F_T^{Max}, \tag{13}$$

where F_T^{Min} and F_T^{Max} are the minimum and maximum flow rate provided by the feed water pump.

2.4. Optimization problem formulation

The main objective of the optimization problem is to minimize the total thermal energy consumption of the facility while assuring the water demand. To achieve this, the manipulated variables available in the real facility are the aperture of the V_m valve ($\delta_m(k)$) and the feed water flow rate ($F_m(k)$) of each MD module. Thus, to formulate the optimization problem, three main things must be considered.

First, the total distillate production must be equal or higher than the water demand, what can be directly included in the optimization problem as a constraint. Nevertheless, as shown in Fig. 1, there is a storage tank available between the consumer and the producer agent. So, the production constraint can be formulated according to the water level of the tank. Note that, the behaviour of this element is like an integrator which allows to filter the water demand, thus smoothing the production constraint.

Second, the total thermal energy consumption of the desalination unit can be directly reduced by turning on as few modules as possible at each moment. This can be achieve by optimally managing the binary variables according to the operating water needs.

Third, when a module is turned on, the total thermal energy it consumes can be reduced by improving its thermal efficiency. In MD processes, one of the most widely used metrics to estimate the thermal efficiency is the STEC [4,10,18]. The STEC is defined as the amount of thermal energy required to produce a volume unit of distillate (kWh/m^3). For a single m-module, it can be calculated as follows:

$$S_m(k) = \frac{c_1 \cdot F_m(k) \cdot \Delta T_m(k)}{d_m(k)}, \tag{14}$$

$$c_1 = \frac{\rho \cdot c_p}{c_f}, \tag{15}$$

where $S_m(k)$ is the STEC of MD m-module, and the rest of variables and constants are defined in Appendix A. It should be noted that to maximize the distillate production (to meet the water needs) and to minimize the STEC in current commercial MD modules, the maximun and minimum feed flow rate must be applied respectively [29]. Thus, the operation of the feed flow rate of each MD module is not trivial, and a tradeoff solution must be taken at each sample time depending on the operating conditions.

According to the above issues, the optimization problem can be formulated as:

$$\min \sum_{m \in \mathcal{M}} \frac{c_1 \cdot F_m(k) \cdot \Delta T_m(k)}{d_m(k)}, \tag{16}$$

subject to, $\forall m \in \mathcal{M}$:

$$d_m(k) = \alpha^d_{m,1}(k) \cdot \delta_m(k) + \alpha^d_{m,2}(k) \cdot F_m(k) + c_2 \cdot (1 - \delta_m(k)), \tag{17}$$

$$\Delta T_m(k) = \alpha^T_{m,1}(k) \cdot \delta_m(k) + \alpha^T_{m,2}(k) \cdot F_m(k), \tag{18}$$

$$\delta_m(k) \cdot F_m^{Min} - F_m(k) \leq 0, \tag{19}$$

$$F_m(k) - \delta_m(k) \cdot F_m^{Max} \leq 0, \tag{20}$$

$$\delta_m(k) \in \{0, 1\}, \tag{21}$$

and the constraints that couple all the MD modules and the consumer and producer agent:

$$\sum_{m \in \mathcal{M}} F_m(k) = F_T(k), \tag{22}$$

$$F_T^{Min} \leq F_T(k) \leq F_T^{Max}, \tag{23}$$

$$\sum_{m \in \mathcal{M}} d_m(k) = d_T(k), \tag{24}$$

$$(d_T(k) - D(k)) \cdot c_3 + L_T(k-1) \geq L^* \tag{25}$$

$$L_T^{Min} \leq L_T(k) \geq L_T^{Max} \tag{26}$$

where c_2 is a large number (i.e., 10_6) used to avoid division by zero in Eq. (16), $D(k)$ is the water demand of the consumer agent, c_3 is the conversion factor, $L_T(k)$ is the water level of the distillate tank, L_T^{Min} and L_T^{Max} are the maximum and minimum level of the tank, and L^* is the setpoint water level of the distillate tank. Note that all the units and description of the variables are available in Appendix A.

In the formulation of the optimization problem, the objective function, Eq. (16), is focused on minimizing the sum of the STEC of each MD module. The summation term allows to minimize the total thermal energy consumption of the whole system, while the STEC calculation allows to enhance the thermal efficiency of the modules turned on at each sampling time. The constraints in Eqs. 17–24 define the model of the system and the physical limits of the manipulated variables. Eq. (25) is related to the production needs, which have been introduced in the problem according to the water level of the distillate tank, as was explained before. Finally, it should be remarked that the disturbances and water demand are known, and therefore, they are fixed in the optimization problem.

Note that, the formulated problem is an MINLP problem due to the nonlinearity of the objective function Eq. (16), and the presence of binary and continuous variables. Regarding the feasibility of the problem, the only constraint that can turn the problem infeasible is Eq. (25). However, as long as the desalination unit and the solar field powering it are well sized according to the water needs the problem will be feasible. In addition, the tank level setpoint can be adapted to the plant operation in the starting of the operation, if the tank starts with level zero. Nevertheless, smoothing techniques could also be applied in this constraint such as the use of slack variables if necessary.

It should be also remarked that the boundary conditions of the problem mainly change according to the operating temperature (temperature at the inlet of the evaporator channel of the MD modules), which depends on solar irradiance. Therefore, the problem must be solved in real time to achieve an optimal operation. However, the nonlinearity of the problem requires a high computational power which prevents the problem from being solved quickly by using MINLP solvers, especially when the number of agents in the array of MD modules is large. Therefore, in the following section we propose an efficient algorithm based on the GBD method for solving this problem.

3. The GBD-based MPC operating strategy

In this section the GBD and the MPC methods are introduced. Then, the MINLP problem presented in the previous section is formulated according to these two methodologies.

3.1. Benders decomposition method

Considering a generic MINLP problem:

$$[x, y] \min f(x, y). \tag{27}$$

$$\text{s.t.} \quad h(x, y) = 0, \tag{28}$$

$$g(x, y) \leq 0, \tag{29}$$

$$x \in \boldsymbol{X} \subseteq \Re^{n_x}, \tag{30}$$

$$y \in \boldsymbol{Y}^{n_y} = \{0, 1\}, \tag{31}$$

the basic idea of the GBD method [30] consists on solving this problem on a iterative way, computing at each iteration an upper and a lower bound in the solution space of the MINLP model. These bounds are obtained by decomposing the overall MINLP problem into two problems: the *master* problem which provides the lower bound, and the *primal* problem which provides the upper bound.

The *primal* problem corresponds to the problem defined in Eqs. 27–31 with the y-variables fixed in a particular solution 0–1, which is denoted by y^l, being l the iteration counter:

$$[x, y] \min f\left(x, y^l\right). \tag{32}$$

$$\text{s.t.} \quad h\left(x, y^l\right) = 0, \tag{33}$$

$$\boldsymbol{g}\left(x, y^l\right) \leq 0, \tag{34}$$

$$x \in \boldsymbol{X} \subseteq \Re^{n_x}. \tag{35}$$

Remark 3.1. *Note that the solution of this primal problem is the global solution for problem (27)-(31).*

At this point, two different cases can be distinguished: feasible *primal*, and infeasible *primal*. If the solution of the *primal* problem is feasible at iteration l, it provides information of: i) the value of x^l, ii) the value of the upper bound, which is the value of $f(x^l, y^l)$, and iii) the value of the optimal Lagrange multipliers vectors $\boldsymbol{\lambda}^l$ and $\boldsymbol{\mu}^l$ related to the set of equality ($\boldsymbol{h}$) and inequality ($\boldsymbol{g}$) constraints respectively. The aforementioned information allows us to formulate the following Lagrange function, which is called the optimallity cut:

$$L^l\left(x, y, \boldsymbol{\lambda}^l, \boldsymbol{\mu}^l\right) = f(x,y) + \boldsymbol{\lambda}^{lT}\boldsymbol{h}(x,y) + \boldsymbol{\mu}^{lT}\boldsymbol{g}(x,y). \tag{36}$$

On the other hand, if the solution of the *primal* problem at iteration l is infeasible, only the constraints of the *primal* problem are considered, and the following optimization problem is formulated in order to identify a feasible solution:

$$\min_{x,\gamma} \gamma \tag{37}$$

$$\text{s.t.} \quad h\left(x, y^l\right) = 0, \tag{38}$$

$$\boldsymbol{g}\left(x, y^l\right) \leq \gamma^l, \tag{39}$$

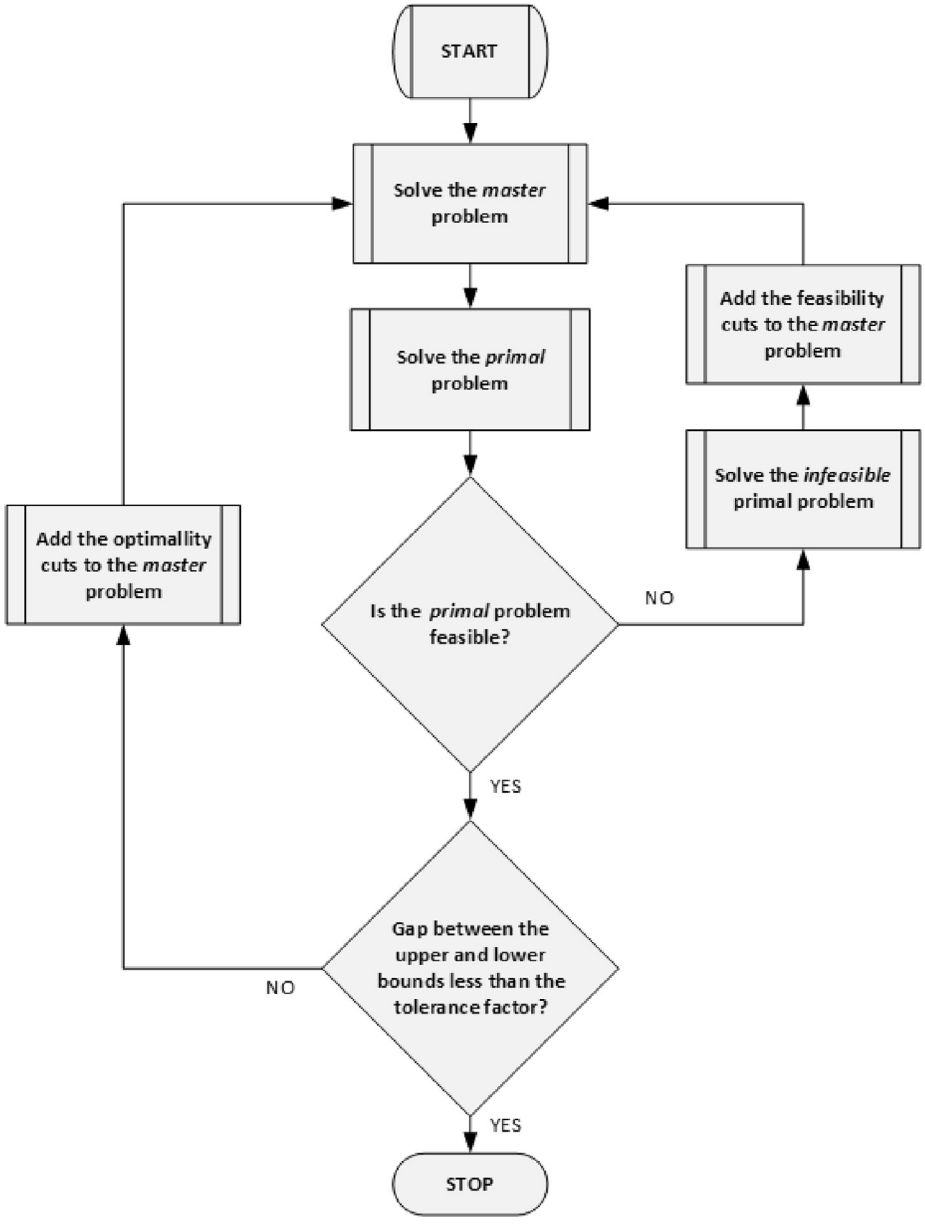

Fig. 4. GBD algorithm.

$$\gamma \geq 0, \tag{40}$$

$$x \in \boldsymbol{X}. \tag{41}$$

The solution of this problem provides information about the Lagrange multipliers related to the equality and inequality constraints, which are denoted in this case as $\overline{\lambda}^l$ and $\overline{\mu}^l$ respectively. These multipliers allows us to formulate the feasibility cut as:

$$\overline{L}^l\left(x, y, \overline{\lambda}^l, \overline{\mu}^l\right) = \overline{\lambda}^{lT}\boldsymbol{h}(x,y) + \overline{\mu}^{lT}\boldsymbol{g}(x,y). \tag{42}$$

Remark 3.2. It should be noted that at each iteration only one cut is generated, depending if the *primal* problem is feasible or infeasible. In addition, the upper bound is generated only if the *primal* problem is feasible.

The *master* problem is defined according to the duality theory being based on the projection of the overall MINLP problem in the *y*-space (see Ref. [30] for more details):

$$[y, \mu_0]\min \mu_0 \tag{43}$$

$$\text{s.t.} \quad \mu_0 \geq L^{l^1}\left(x^{l^1}, y, \lambda^{l^1}, \boldsymbol{\mu}^{l^1}\right)\ l^1 = 1, \ldots, L^1, \tag{44}$$

$$0 \geq \overline{L}^{l^2}\left(x^{l^2}, y, \overline{\lambda}^{l^2}, \overline{\boldsymbol{\mu}}^{l^2}\right)\ l^2 = 1, \ldots, L^2, \tag{45}$$

where L^1 and L^2 are the last iteration counters at which the optimallity and feasibility cuts were updated.

Remark 3.3. *The master problem is equivalent to the MINLP (27)-(31). Also, the value of the variable μ_0 is the value of the lower bound.*

The whole algorithm is solved on an iterative way according to the flow-chart presented in Fig. 4. The iterations terminate when the gap between the upper and the lower bound is lower than a given tolerance factor, which is, $UB \leq LB + \varepsilon$, where *UB* and *LB* are the upper and lower bounds respectively and ε is a tolerance factor.

3.2. Model Predictive Control

The MPC strategy is one of the most widespread control methodologies used in both industry and academia. The MPC is not an explicit control technique, but rather comprises a wide range of control methods based on the use of a model of the system for obtaining the control actions by minimizing an objective function [31]. Specifically, the procedure used in MPC controllers is given by (see Fig. 5):

1. The outputs of the process for a given prediction horizon *N*, are predicted at each time *k* by using a model of the system. The predicted outputs, denoted by $\widehat{z}(k+j|k)$ for $j = 1, \ldots, N$, depend on past outputs, inputs and disturbances, and on the value of future control actions $u(k+j-1|k)$ for $j = 1, \ldots, N$. Note that the notation $(k+j|k)$ is related to the predicted value of a variable at the instant time $k+j$, calculated with the information available at instant *k*.
2. The set of future control actions is calculated by minimizing a determined objective function.
3. The control action $u(k|k)$ is sent to the system while the rest of control signals are rejected because at the next sampling time, $\widehat{z}(k+1)$ will be known, allowing to repeat the first step with the updated information. This methodology is known as the receding horizon concept.

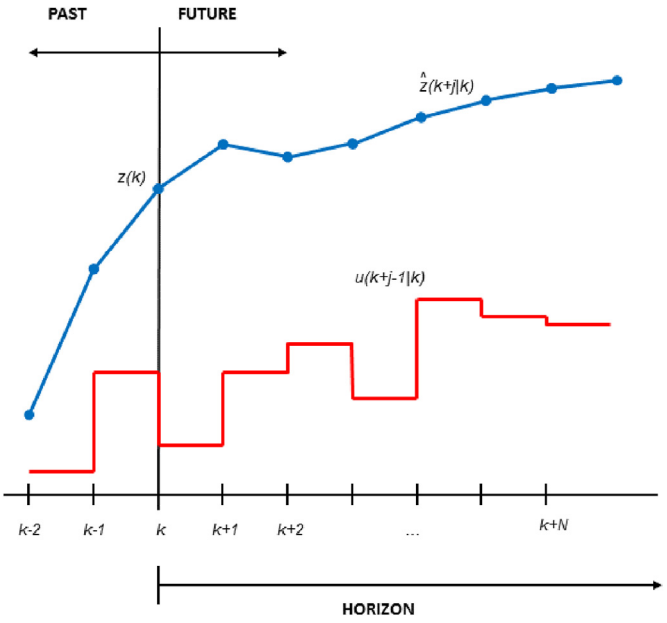

Fig. 5. MPC strategy.

It should be remarked that, the application of the MPC technique in the problem concerning this work is specially suitable due to the presence of the distillate tank. This method allows us to predict the level of the tank taking into account future water demands, and therefore, to induce the optimal management and high performance of the desalination plant.

3.3. The GBD-based MPC algorithm

Once both techniques have been introduced, the decomposition of the overall MINLP problem (see Eqs. 16–25) is formulated according to them. It should be pointed out that the problem treated in this work has the same structure of the generic problem presented in Section 3.1, with a set of binary, δ_m, $\forall m \in \mathscr{M}$, and continuous variables, F_m, $\forall m \in \mathscr{M}$. Therefore, the *primal* problem will be the projection of the overall MINLP problem in the F_m-space, while the *master* problem will be the projection of the problem in the δ_m-space.

It should be also taken into account that the variables $\alpha^d_{m,1}$, $\alpha^d_{m,2}$, $\alpha^T_{m,1}$ and $\alpha^T_{m,2}$ can be predicted along the prediction horizon, as they depend on the measurable temperatures (see Section 2.3).

Thus, the feasible *primal* problem can cast:

$$\min \sum_{j=1}^{N} \sum_{m \in \mathscr{M}} \frac{c_1 \cdot F_m(k+j-1|k) \cdot \Delta \widehat{T}_m(k+j|k)}{\widetilde{d}_m^{\,l}(k+j-1|k)}, \tag{46}$$

subject to, $\forall m \in \mathscr{M}$ and $j = 1, \ldots, N$:

$$\begin{aligned} \widehat{d_m}(k+j|k) = {} & \widehat{\alpha}^d_{m,1}(k+j|k) \cdot \delta^l_m(k+j-1|k) \\ & + \widehat{\alpha}^d_{m,2}(k+j|k) \cdot F_m(k+j-1|k), \end{aligned} \tag{47}$$

$$\widetilde{d}_m^{\,l}(k+j-1|k) = \widehat{d}_m^{\,l-1}(k|k) + c_2 \cdot \left(1 - \delta^l_m(k+j-1|k)\right), \tag{48}$$

$$\Delta\widehat{T}_m(k+j|k) = \widehat{\alpha}^T_{m,1}(k+j|k)\cdot\delta^l_m(k+j-1|k) + \widehat{\alpha}^T_{m,2}(k+j|k)\cdot F_m(k+j-1|k), \tag{49}$$

$$\delta^l_m\Big(k+j-1|k)\cdot F^{Min}_m - F_m(k+j-1|k\Big) \le 0, \tag{50}$$

$$F_m\Big(k+j-1|k) - \delta^l_m(k+j-1|k\Big)\cdot F^{Max}_m \le 0, \tag{51}$$

$$F^{Min}_T \le F_T(k+j-1|k) \le F^{Max}_T, \tag{52}$$

$$(\widehat{d_T}(k+j|k) - \widehat{D}(k+j|k))\cdot c_3 + \widehat{L_T}(k+j-1|k) \ge L^*, \tag{53}$$

$$L^{Min}_T \le L_T(k+j|k) \ge L^{Max}_T \tag{54}$$

and

$$\sum_{j=1}^{N}\sum_{m\in\mathscr{M}} F_m(k+j-1|k) = F_T(k+j-1|k), \tag{55}$$

$$\sum_{j=1}^{N}\sum_{m\in\mathscr{M}} \widehat{d_m}(k+j|k) = \widehat{d_T}(k+j|k). \tag{56}$$

As can be seen, for the calculation of the STEC in Eq. (46), an estimation of the distillate production, $\widetilde{d_m}^l$, is used instead of the actual distillate production, $\widehat{d_m}(k+j|k)$. One should highlight that the objective function of the overall MINLP problem, Eq. (16), can be rewritten as follows, by combining it with Eq. (18):

$$\min \sum_{m\in\mathscr{M}} \frac{c_1\cdot F_m(k)\cdot\alpha^T_{m,1}(k)\cdot\delta(k)}{d_m(k)} + \sum_{m\in\mathscr{M}} \frac{c_1\cdot\alpha^T_{m,2}(k)\cdot F_m(k)^2}{d_m(k)}, \tag{57}$$

where for $d_m(k)>0$, the right part of the equation is convex whereas the left part is quasi-convex. The estimation of the distillate production allows us to eliminate this quasi-convex part in the objective function, rendering the objective function convex. Note that, the estimation is updated at each iteration of the algorithm as shown in Eq. (48), where $\widetilde{d_m}^{l-1}(k|k)$ is the value of $\widehat{d_m}(k|k)$ calculated in the previous iteration $l-1$. In this way, in the last iterations, $\widetilde{d_m}^l$ reaches a static value which is the optimum or very close to the optimum, ensuring the stability of the solution. In addition, by using the estimation, Eq. (46) can be formulated as:

$$\min \sum_{j=1}^{N}\sum_{m\in\mathscr{M}} \frac{c_1\cdot F_m(k+j-1|k)\cdot\widehat{\alpha}^T_{m,1}(k+j|k)\cdot\delta^l_m(k+j-1|k)}{\widetilde{d_m}^l(k+j-1|k)} + \sum_{j=1}^{N}\sum_{m\in\mathscr{M}} \frac{c_1\cdot\widehat{\alpha}^T_{m,2}(k+j|k)\cdot F_m(k+j-1|k)^2}{\widetilde{d_m}^l(k+j-1|k)}, \tag{58}$$

where all the parameters involved in the equation are constants, except $F_m(k+j-1|k)$, what enables the problem to be solved with a simple QP solver.

The infeasible *primal* problem can be formulated as:

$$\min \sum_{j=1}^{N}\gamma(k+j), \tag{59}$$

subject to, $\forall m\in\mathscr{M}$ and for $j=1,\ldots,N$:

$$\widehat{d_m}(k+j|k) - \Big[\widehat{\alpha}^d_{m,1}(k+j|k)\cdot\delta^l_m(k+j-1|k) \widehat{\alpha}^d_{m,2}\Big(k+j|k)\cdot F_m(k+j-1|k\Big)\Big)\Big] - \gamma(k+j) \le 0, \tag{60}$$

$$-\widehat{d_m}\Big(k+j\Big|k\Big) + \Big[\times\Big(\widehat{\alpha}^d_{m,1}\Big(k+j\Big|k\Big)\cdot\delta^l_m\Big(k+j-1\Big|k\Big) + \widehat{\alpha}^d_{m,2}(k+j|k)\cdot F_m(k+j-1|k) \times\Big] - \gamma(k+j) \le 0, \tag{61}$$

$$\delta^l_m\Big(k+j-1|k)\cdot F^{Min}_m - F_m(k+j-1|k\Big) - \gamma(k+j) \le 0, \tag{62}$$

$$F_m\Big(k+j-1|k) - \delta^l_m(k+j-1|k\Big)\cdot F^{Max}_m - \gamma(k+j) \le 0, \tag{63}$$

$$F^{Min}_T - F_T(k+j-1|k) - \gamma(k+j) \le 0, \tag{64}$$

$$F_T(k+j-1|k) - F^{Max}_T - \gamma(k+j) \le 0, \tag{65}$$

$$L^* - [(\widehat{d_T}(k+j|k) - \widehat{D}(k+j|k))\cdot c_3 + \widehat{L_T}(k+j-1|k)] - \gamma(k+j) \le 0, \tag{66}$$

$$L^{Min}_T - L_T(k+j-1|k) - \gamma(k+j) \le 0, \tag{67}$$

$$L_T(k+j-1|k) - L^{Max}_T - \gamma(k+j) \le 0, \tag{68}$$

and

$$\sum_{j=1}^{N}\sum_{m\in\mathscr{M}} F_m(k+j-1|k) - F_T(k+j-1|k) - \gamma(k+j) \le 0, \tag{69}$$

$$F_T\left(k+j-1|k) - \sum_{j=1}^{N}\sum_{m\in\mathscr{M}} F_m(k+j-1|k\right) - \gamma(k+j) \le 0, \tag{70}$$

$$\sum_{j=1}^{N}\sum_{m\in\mathscr{M}} \widehat{d_m}(k+j|k) - \widehat{d_T}(k+j|k) - \gamma(k+j) \le 0, \tag{71}$$

$$\widehat{d_T}\left(k+j|k) - \sum_{j=1}^{N}\sum_{m\in\mathscr{M}} \widehat{d_m}(k+j|k\right) - \gamma(k+j) \le 0. \tag{72}$$

This problem is proposed only with the constraints of the feasible *primal* problem according to the GBD theory. Also, the equality constraints have been rewritten as inequality constraints for the sake of simplicity in the implementation of the method. It is worth noting that, this optimization problem can be worked out with an LP solver.

Finally, the *master* problem is written as:

$$\min \sum_{j=1}^{N} \mu_0(k+j), \tag{73}$$

subject to, $\forall j = 1...N$, $l^1 = 1,\ldots,L^1$, and $l^2 = 1,\ldots,L^2$

$$\mu_0(k+j) \geq \sum_{m\in M} \lambda_{1,m}^{l^1}(k+j)\cdot\left[F_m^{l^1}(k+j-1|k) - \delta_m(k+j-1|k)\cdot F_m^{Max}\right] + \sum_{m\in M} \lambda_{2,m}^{l^1}(k+j)\cdot\left[\delta_m\left(k+j-1|k\right)\cdot F_m^{Min} - F_m^{l^1}(k+j-1|k)\right] + J_{primal}^{l^1}(k+j|k), \tag{74}$$

$$0 \geq \sum_{m\in M} \overline{\lambda}_{1,m}^{l^2}\left(k+j\right)\cdot\left[\widehat{d}_m^{l^2}\left(k+j\middle|k\right) - \left(\widehat{\alpha}_{m,1}^{d}\left(k+j\middle|k\right)\cdot\delta_m\left(k+j-1\middle|k\right) + \widehat{\alpha}_{m,2}^{d}\left(k+j\middle|k\right)\cdot F_m^{l^2}\left(k+j-1\middle|k\right)\right)\times\right] + \sum_{m\in M} \overline{\lambda}_{2,m}^{l^2}\left(k+j\right)\cdot\left[-\widehat{d}_m^{l^2}\left(k+j\middle|k\right) + \left(\widehat{\alpha}_{m,1}^{d}(k+j|k)\cdot\delta_m(k+j-1|k) + \widehat{\alpha}_{m,2}^{d}\left(k+j|k\right)\cdot F_m^{l^2}(k+j-1|k)\right)\right] + \sum_{m\in M} \overline{\lambda}_{3,m}^{l^2}(k+j)\cdot\left[F_m^{l^2}(k+j-1|k) - \delta_m(k+j-1|k)\cdot F_m^{Max}\right] + \sum_{m\in M} \overline{\lambda}_{4,m}^{l^2}(k+j)\cdot\left[\delta_m\left(k+j-1|k\right)\cdot F_m^{Min} - F_m^{l^2}(k+j-1|k)\right], \tag{75}$$

where $J_{primal}^{l^1}(k+j|k)$ is the value of the objective function of the feasible *primal* problem, $\lambda_{1,m}^{l^1}(k+j)$ and $\lambda_{2,m}^{l^1}(k+j)$ are the Lagrange multipliers of the constraints Eqs. (50) and (51) at iteration l^1, obtained from the solution of the feasible *primal* problem, and $\overline{\lambda}_{1,m}^{l^2}(k+j)$, $\overline{\lambda}_{2,m}^{l^2}(k+j)$, $\overline{\lambda}_{3,m}^{l^2}(k+j)$ and $\overline{\lambda}_{4,m}^{l^2}(k+j)$ are the ones related to Eqs. (60)–(63) obtained from the solution of the infeasible *primal* problem at iteration l^2. Observe also that Eq. (74) is related with the optimallity cuts and Eq. (75) with the feasibility ones. It should be also remarked that this problem is an MILP problem that can be worked out with a suitable algorithm.

The algorithm is solved according to the resolution method presented in Fig. 4. In addition, Fig. 6 shows the variables shared between problems at each iteration. Note that, the prediction of variables $\widehat{\alpha}_{m,1}^{d}$, $\widehat{\alpha}_{m,2}^{d}$, $\widehat{\alpha}_{m,1}^{T}$ and $\widehat{\alpha}_{m,2}^{T}$ is global information, and, therefore, it is known for all the problems.

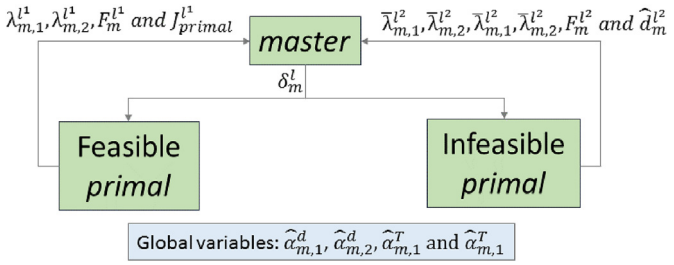

Fig. 6. Information shared between problems. The variables shared are $\forall m \in \mathcal{M}$. Observe that the MPC nomenclature has not been included in the figure for the sake of simplicity.

4. Results and discussion

4.1. Case study

The case study adopted in this work is based on two real facilities located in Almería (southeast Spain). On the one hand, for the desalination unit, the SMD facility of the Plataforma Solar de Almería (PSA, www.psa.es) was used as reference [4]. Among the different commercial MD modules useable at PSA, the Aquastill unit and the Solar Spring one were chosen (see Fig. 7) to be part of the array of MD modules. These two modules were selected since they have different behaviours in terms of distillate production and thermal efficiency, what adds complexity to the problem. The Aquastill module has a lower thermal energy consumption and a higher distillate production than the Solar Spring one, as was stated in Ref. [29]. One should bear in mind that the models of these two modules were already presented and validated in literature in Ref. [10,18] for the Solar Spring and Aquastill module respectively. These models can be formulated according to the generic method described in Section 2.2 and 2.3. Table 1 presents the value of the polynomial coefficients of the RSM models of each MD module.

On the other hand, a greenhouse was selected as consumer agent. Note that the combination of greenhouses and SMD plants is a potential industrial application of MD technology [29], and of thermal powered desalination technologies in general [32]. Besides, a greenhouse presents a variable water demand according to the meteorological conditions [32], which makes the use of optimal management techniques in the desalination unit essential. In this way, a multi-span "Almeria-type" greenhouse (see Fig. 8) located at the Experimental Station of the Cajamar Foundation (also in the southeast of Spain) was employed in the simulations. The dynamical model of the greenhouse, the validation of the model, and a detailed description of the greenhouse environment were presented in [33]. Note that in this model, the water demand is decided according to the crop transpiration flux, which relates to the amount of water lost by the plants during the transpiration process and must be recovered by irrigation.

4.2. Simulation set-up

The simulations were performed following the scheme deployed in Fig. 9. As can be observed, the real facility in the simulation loop was composed by the model of the array of MD modules, the model of the heat exchanger connecting the solar field and the desalination unit, and the model of the greenhouse. Note that, for these two last elements, the same models from Ref. [29] were employed. Also, in the simulations, the array of MD modules was composed by the same number of Solar Spring and Aquastill modules, placing the Solar Spring modules in the odd numbers of the array and the Aquastill modules in the even ones. In addition, the maximum and minimum feed flow rate (F_m^{Min} and F_m^{Max}) of each MD module was stated as 400 and 600 L/h respectively, in accordance with the operating range of these commercial MD modules (see Ref. [10,18] for more details). The minimum range of the feed water pump (F_T^{Min}) was fixed at zero and the maximum (F_T^{Max}) at $N_m \cdot 600$, where N_m is the number of MD modules in the array.

It should be highlighted that, real data were used to feed the models mentioned above, what adds reliability to the simulations. In order to simplify the simulation loop, a temperature profile at the entrance of the heat exchanger was used ($T_{hs,in}$ in Fig. 9) instead of including the complete heat generation model. These profiles were obtained by simulating the complete model of the heat generation

Fig. 7. Commercial MD modules at PSA. From left to right: Solar Spring and Aquastill modules.

Table 1
Polynomial coefficients of the RSM models of the Aquastill and Solar Spring modules.

Coefficient	Module	
	Aquastill	Solar Spring
p_1 (L/h)	3.24	−10.88
p_2 (L/(h·°C))	0.072	0.24
p_3 (L/(h·°C))	−0.4896	−0.18
p_4 (−)	−0.024	−0.01
p_5 (1/°C)	0.0096	0.0006
p_6 (°C)	−0.739	−0.2018
p_7 (−)	0.078	0.1385
p_8 (−)	−0.067	−0.158
p_9 (h/(L·°C))	0.0019	0.0049

circuit (which was presented in Ref. [26]) with real meteorological data, similar to the ones used as input of the greenhouse model, and with the operational strategy presented in Ref. [7]. The model of the greenhouse was directly fed with real meteorological data (see Fig. 9), which were obtained from Experimental Station of the Cajamar Foundation. It should be remarked that, in the prediction model of the MPC strategy, the meteorological conditions as well as inlet temperature at the hot side of the heat exchanger ($T_{hs,in}$) were maintained constant along the prediction horizon. Also, the feed temperature (T_{feed}) was fixed at 20 °C (average temperature of the Mediterranean sea).

In the simulation loop, the MPC controller received the states from the different models comprising the real simulating facility, and sent the corresponding control action $\boldsymbol{u}$ (i.e., δ_m and F_m, $\forall m \in \mathscr{M}$) to the array of MD modules at each sampling time. The sampling time of the system was established in 10 min according to the representative time constant of the greenhouse water demand and the desired closed loop behaviour [29].

All the simulations were performed using MATLAB code [34] (MATLAB version 2018a) running on a PC with an Intel Core i5-6500T CPU 2.50 GHz with 8 GB of RAM. Moreover, it should be noted that the overall MINLP problem was solved with the BARON solver (version 1.88) [35], whereas the optimization problems of the GBD method were solved with the CPLEX solver [36] (version 12.6.1).

4.3. Study of efficiency of the proposed algorithm

One of the main benefits of the developed management method is that simpler optimization problems, such as QP, LP and MILP, are

Fig. 8. Greenhouse environment. From left to right and from top to bottom: the greenhouse, the dropper and the tomato crop lines.

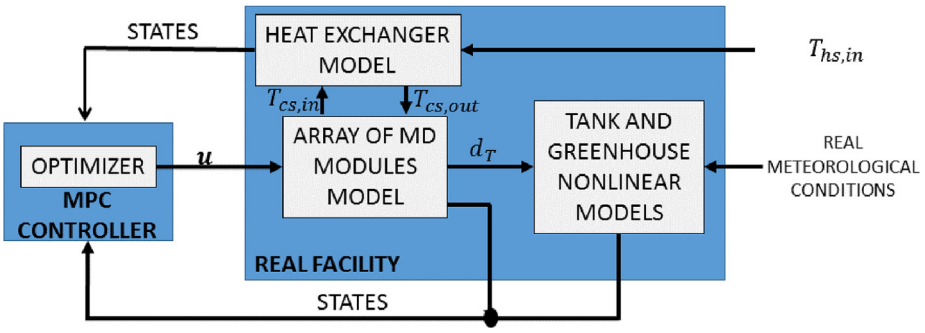

Fig. 9. Simulation scheme.

Table 2
Results reached with each resolution method when increasing the number of MD modules in the array. V-obj is the value of the objective function.

Number of MD units	GBD algorithm		MINLP algorithm	
	Time [s]	V-obj [kWh/m$_3$]	Time [s]	V-obj [kWh/m$_3$]
4	0.29	112.25	1.50	112.25
8	0.29	112.30	1.60	112.28
16	0.30	224.50	3.77	224.50
32	1.56	382.40	102.23	382.06
64	5.67	455.20	1619.72	451.55

solved instead of an overall MINLP one. This fact directly influences the time spent in reaching an optimal solution of the problem. So that, in this section, the GBD based method and MINLP solver are analyzed in terms of computational time. To do this, several simulations were carried out, increasing the number of agents (i.e., the number of MD modules in the array). The time spent by each resolution method to work out the overall MINLP problem in a single sampling time was measured.

Table 2 summerizes the results of the different simulations and Fig. 10 graphically represents these results. As can be observed, five cases were simulated, with 4, 8, 16, 32 and 64 MD modules. For the two first cases, in which the number of MD modules was small, both algorithms solved the problem quickly, reaching the same value in the objective function. In the third case, the time required by the MINLP solver was doubled in comparison with the two first cases, whereas the one of the GBD based approach remained almost constant. In the two last cases, the time spent by the MINLP solver increased exponentially (see Fig. 10). Note that with 64 MD modules, the time spent by the MINLP solver is much longer than the system's sampling time (600 s). This fact means that the MINLP solver cannot be used when considering a plant equal or larger than that size. It is worth noting that, this also happens when using the MPC strategy with long prediction horizons, since for the purpose of the optimization problem, it has the same effect as using a large number of MD modules in the array.

Finally, it should be remarked that the GBD algorithm reached almost the same values that the global MINLP solver in the objective function (see Table 2), which indicates convergence to optimal solutions. The slight differences are due to the value chosen for $\varepsilon = 0.5$. This value was taken considering the trade-off between resolution time and accuracy. Nevertheless, it should be remarked that the aforementioned differences are not representative in comparison to the magnitude of the objective function.

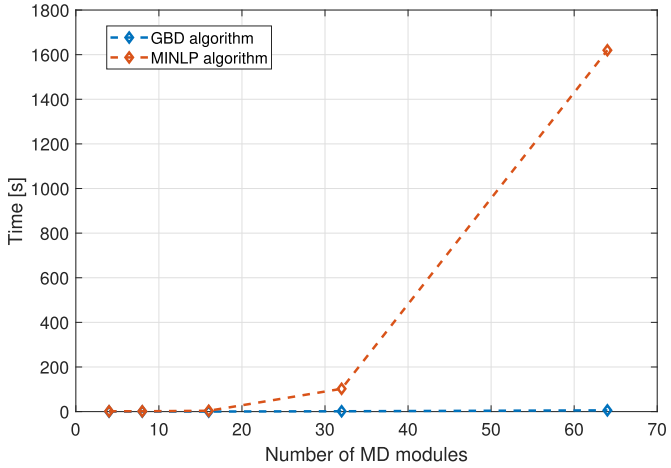

Fig. 10. Results reached with each resolution method when increasing the number of MD modules in the array.

4.4. Simulation study

To assess the running of the proposed algorithm during a daily operation of the facility, different tests were executed with several values of the prediction horizon N. For these tests, the desalination unit was configured with four MD modules, and the greenhouse with a size of 308 m^2, as in the tests performed in Ref. [29]. It should be highlighted that, this small scale plant was chosen for being representative of the system and allowing to visualize the results on a easy way. Besides, the tests were performed with meteorological data from the Experimental Station of the Cajamar Foundation on the day of June 6th, 2017. It should be also remarked that, as the array of modules included identical modules (i.e., two of Aquastill and two of Solar Spring), a term in the objective function was added to prevent chattering problems in the switching on and off of the modules between one sampling time and the next. The term added to the *primal* and *master* problems consisted of $\sum_{m\in\mathcal{M}} (\delta_m(k+j-1|k) - \delta_m(k+j-2|k))^2$.

Figs. 11 and 12 show two representative tests with $N = 1$ and $N = 4$ respectively. Please note that the global irradiance has not been included in the figures for the sake of simplicity. However, it should be remarked that the dynamical behaviour of both, the inlet temperature at the hot side of the heat exchanger ($T_{hs,in}$) and the water demand (D) depends directly on this variable. In this way, in the simulations, the water consumption of the greenhouse was maximum around the solar midday (see Fig. 11-4,12-(4)). Nevertheless, $T_{hs,in}$ reached the maximum value later (see Fig. 11-1,12-(1)) because of the volume of water accumulated in the solar field

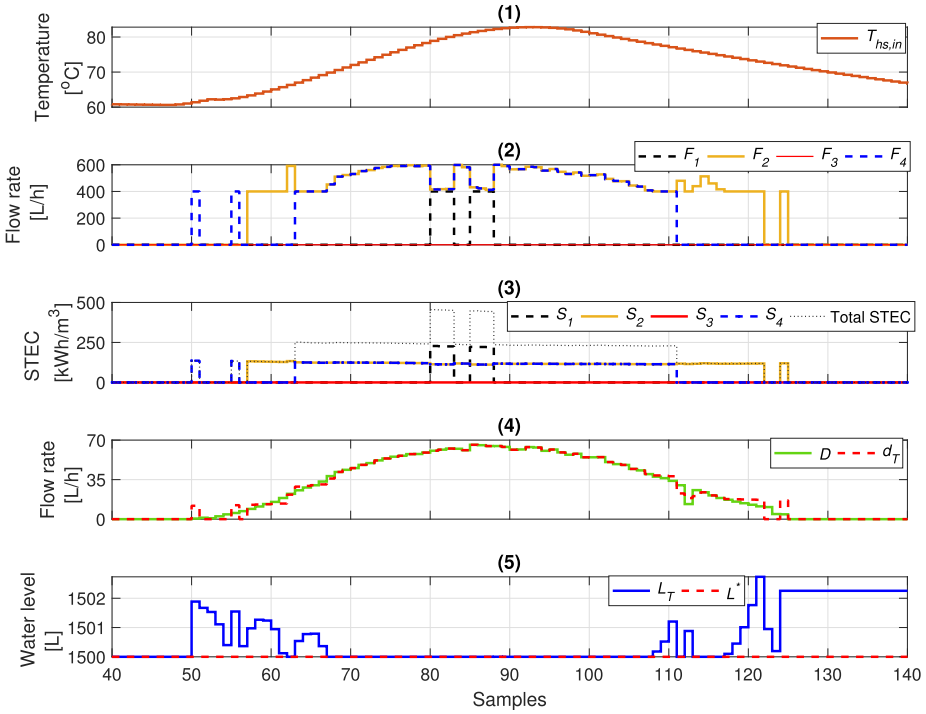

Fig. 11. Simulation results obtained during a daily operation of the plant with the proposed approach with $N = 1$. (1) Temperature at the inlet of the hot side of the heat exchanger ($T_{hs,in}$), (2) feed flow rates of each MD module included in the desalination unit (F_1, F_2, F_3 and F_4), (3) STEC of each module (S_1, S_2, S_3 and S_4) and total STEC of the whole system (total STEC), (4) water demand (D) and total distillate production (d_T), and (5) actual water level of the tank (L_T) and desire level (L^*).

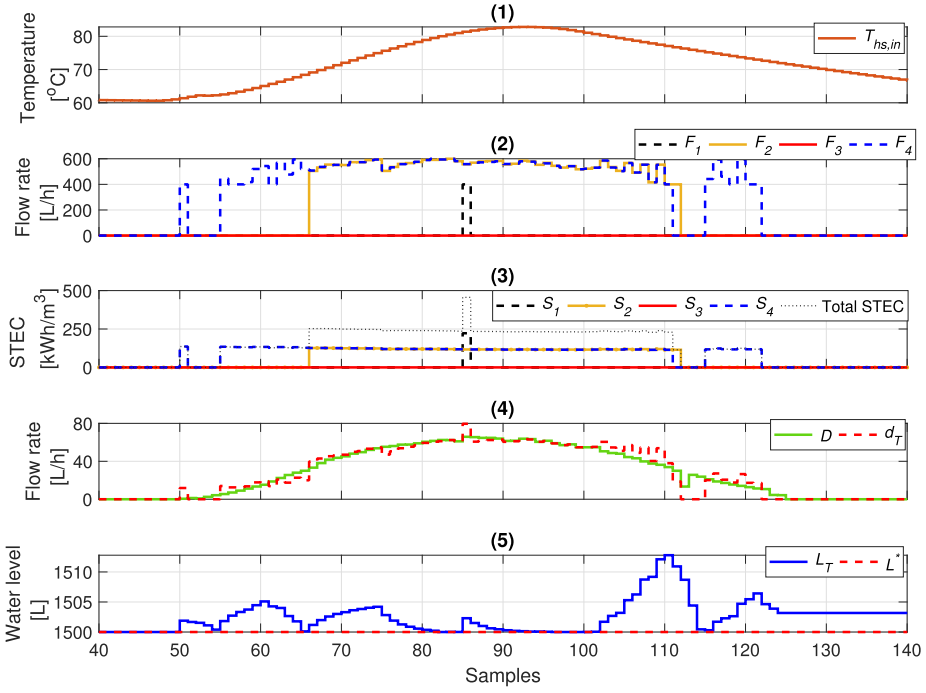

Fig. 12. Simulation results obtained during a daily operation of the plant with the proposed approach with $N = 4$. (1) Temperature at the inlet of the hot side of the heat exchanger ($T_{hs,in}$), (2) feed flow rates of each MD module included in the desalination unit (F_1, F_2, F_3 and F_4), (3) STEC of each module (S_1, S_2, S_3 and S_4) and total STEC of the whole system (total STEC), (4) water demand (D) and total distillate production (d_T), and (5) actual water level of the tank (L_T) and desire level (L^*).

storage tank (see Fig. 1).

As can be observed in Fig. 11-5,12-(5), the simulations started with a level in the distillate tank equal to the setpoint level, which was set as 1500 L. Therefore, as soon as the water demand was higher than zero, the controller turned on one of the Aquastill modules (which are the most efficient) at its minimum feed flow rate, 400 L/h (see Fig. 11-2,12-(2)). This fact caused the level of the tank to increase as the production was higher than the demand,

and therefore, at the next sampling time, the module was turned off again. From sample 55, there were differences between the performance of the management method in both tests, which were caused by the value of the prediction horizon.

In general terms, it can be seen how the controller with $N = 1$ (see Fig. 11), which means to take into account a prediction of 10 min at each sampling time, used more modules than in the case with $N = 4$ because of the low prediction horizon. This was especially relevant around midday when the controller with $N = 1$ (see Fig. 11-(2)) turned on one of the less efficient modules twice for three and four sampling times respectively. Regarding the controller with $N = 4$ (which means to consider a prediction of 40 min at each sampling time), it can be seen that (see Fig. 12), thanks to a longer prediction horizon, the controller anticipated the increase in water demand better. In this way, it augmented the production of one of the aquastill modules progressively by increasing its feed flow rate (see Fig. 12-(2) from sample 55 to sample 66). Then, it turned on the other Aquastill module, and in the solar midday, it activated one of the Solar Spring modules only once during a single sampling time. Note that, the advantages achieved by operating the facility this way were directly reflected in the thermal energy consumption of the desalination unit. This fact can be seen in Fig. 11-3,12-(3). Observe as the total STEC (which is the sum of the STEC of the four MD modules, the value of the objective function) in the case with $N = 1$ was higher than the one of the controller with $N = 4$ from sample 62 to sample 66, due to the use of two MD modules. This happened also in the solar midday from sample 80 to 88.

Moreover, Table 3 summerizes the results obtained in the operation with different values of N. Observe as both, the total thermal energy consumption and the mean STEC of the operation decreased as the prediction horizon increased from $N = 1$ to $N = 4$. On the contrary, for higher horizons, the value of these two metrics was worse. This was caused by errors in the predictions. It is worth noting that, the water demand decreased at the end of the solar day according to the global irradiance. However, the water demand was fixed constant along the prediction horizon. This caused the production to be greater than necessary, what penalized the thermal energy consumption of the desalination unit when using a larger prediction horizon than $N = 4$.

4.5. Comparison with previous and non-optimal approaches

In this section, three representative days with different meteorological conditions were used to compare a manual operation, an operation performed with the approach presented in Ref. [29], and an operation with the management method presented in this paper. The data corresponded to July 10th, 2017, June 6th, 2017 and March 4th, 2015 (test 1, 2 and 3 respectively). The first day was a sunny day, similar to the one presented in the previous section but with a higher level of irradiance (see the cumulative global irradiance, CTI, for test 1 in Table 4). This fact caused the water consumption of the greenhouse to be higher, and the desalination unit to operate around 80% of its capacity to cover the needs when the demand was maximum. The second day corresponded to the test presented in the previous section. Note that, in that test, the water needs required the operation of the desalination unit to be around 50% of its capacity in the moments of maximum consumption. The third test was a cloudy day, so that, the water requirements of the greenhouse were low, which could be covered with the operation of the desalination unit at less than 30% of its capacity.

It should be remarked that in both, the manual method and the one presented in Ref. [29], the four modules included in the desalination unit were turned on as long as the water demand was higher than zero. On the one hand, the manual operation were performed with the feed flow rate of each MD module fixed at 500 L/h. On the other hand, with the method presented in Ref. [29], the feed flow rate of each MD module was manipulated according to the water needs trying to reduce the STEC.

Table 4 shows the results obtained with each technique. As can be seen, in the first test, the manual procedure required 1213.57 kWh of thermal energy, whereas the approach presented in Ref. [29] 982.48 kWh (see Table 4). The amount of thermal energy saved by using the proposed technique is considerable, around 65 and 55% with respect to the manual operation and the one performed with procedure presented in Ref. [29] respectively. This was the result by two main facts. First, the total distillate production (1015.10 L) was almost totally adjusted to the water demand (1013.03 L), which was achieved by manipulating the number of MD modules turned on at each sampling time according to the water needs. This allowed the controller to use only the most efficient MD modules at the beginning and at the end of the day (when the water demand was low), thus saving a large amount of thermal energy. Second, when a module was turned on, its STEC was minimized, which also allowed to reduce the total thermal energy consumption. In the second test, the performance was similar to the previous one, but in this case, as the water needs were lower, the amount of thermal energy saved was even higher, around 85 and 80% in comparison with the manual procedure and the method proposed in Ref. [29] respectively. In the third test, the level of irradiance was lower, and therefore, the water requirements too. In this case, the benefits attained by using the proposed technique were greater as the water needs could be met using only the most efficient modules in the array during the whole operation. Thus, less than the 5% of the thermal energy required by the manual operation and the one performed with the approach in Ref. [29] was used with the application of the proposed method.

Table 3
Results obtained in the operation with different values of N. DP is the total distillate production, M-STEC is the mean STEC of the MD facility during the operation and TTEC is the total thermal energy consumption.

	DP [L]	M-STEC [kWh/m^3]	TTEC [kWh]
$N = 1$	691.86	261.03	180.59
$N = 2$	692.19	258.54	178.95
$N = 3$	692.94	257.80	178.78
$N = 4$	693.51	257.22	178.38
$N = 5$	694.26	258.11	179.19
$N = 6$	695.36	259.30	180.30

5. Conclusions

This paper proposes a general optimal operating strategy aimed at reducing the total thermal energy consumption of commercial membrane distillation facilities. The proposed approach is based on the Generalized Benders Decomposition (GBD) method, which allows us to solve the MINLP optimization problem associated to the management of the facility in a simple and efficient way. In addition, a Model Predictive Control (MPC) strategy is employed to reflect the operational strategy in real time. The developed method was applied in a practical case study, in which an SMD plant was connected to a greenhouse with a variable water demand. The obtained results allow us to draw the following conclusions:

- The developed strategy can be applied in any commercial desalination facility based on membrane distillation as long as the MD modules are modelled with the RSM method.

Table 4
Comparison of results. CTI is the cumulative global irradiance, WD is the total water demand, DP is the total cumulative distillate production, M-STEC is the mean STEC (thermal efficiency) of the MD facility during the operation and TTEC is the total thermal energy consumption.

	Test 1			Test 2			Test 3		
	CTI = 29951 [kJ/m^2]			CTI = 26488 [kJ/m^2]			CTI = 17406 [kJ/m^2]		
	WD = 1013.03 [L]			WD = 690.95 [L]			WD = 210.62 [L]		
	DP	M-STEC	TTEC	DP	M-STEC	TTEC	DP	M-STEC	TTEC
	[L]	[kWh/m^3]	[kWh]	[L]	[kWh/m^3]	[kWh]	[L]	[kWh/m^3]	[kWh]
Manual operation	1589.70	763.40	1213.57	1312.60	831.33	1091.20	1095.70	859.25	941.48
Procedure proposed in [29]	1383.34	710.23	982.48	1152.40	805.42	928.16	957.15	832.17	796.51
Proposed approach	1015.10	426.99	433.43	693.51	257.22	178.38	211.46	139.82	26.04

- The efficiency analysis performed showed as the developed technique reaches almost the same results of an MINLP solver. However, the resolution time was considerable improved. For example, for a facility with 64 MD modules, an MINLP solver required 1619.72 s for solving the problem in a single sampling time, whereas the proposed approach only 5.67 s.
- Regarding the operation, the proposed method was able to manage the facility optimally when coupled to a variable water demand, deciding at each sampling time the number of MD modules turned on and their operating feed flow rate, reducing the total thermal energy consumption of the desalination unit and ensuring the water needs.
- The comparison performed with a manual operation and with a previous proposed approach in literature showed how, in a sunny day, around the 65 and 55% of the thermal energy used by these methods can be saved with the application of the developed technique. In a cloudy day, the benefits are even higher, so that, the proposed approach used less than 5% of the energy required by the other operating methods. These improvements could be very important for both the design of SMD commercial facilities and their daily operation, especially if non-renewable sources are also taken into account to feed the desalination unit or as a backup for cloudy days.

CRediT authorship contribution statement

Juan D. Gil: Conceptualization, Software, Investigation, Writing - original draft. **Paulo R.C. Mendes:** Methodology, Investigation, Writing - review & editing. **E. Camponogara:** Methodology, Writing - review & editing. **Lidia Roca:** Conceptualization, Resources, Writing - review & editing. **J.D. Álvarez:** Conceptualization, Writing - review & editing. **Julio E. Normey-Rico:** Supervision, Writing - review & editing.

Acknowledgements

This work has been funded by the National R + D + i Plan Project DPI2017-85007-R of the Spanish Ministry of Science, Innovation and Universities and ERDF funds. Juan D. Gil is supported by an FPI Fellowship from the University of Almería. Julio E. Normey-Rico thanks CNPq under project 305785/2015-0. Work developed during the posdoc stay of P. Mendes at UFSC.

Appendix A. Nomenclature

Variable	Description	Units
c_1	Constant used in the STEC calculation	kWh/^{o}C.m$_3$
c_2	Constant for the GBD algorithm	10^6
c_3	Conversion factor for the tank level calculation	0.16 h
c_f	Conversion factor to the STEC	$3.6{\cdot}10^6$ s·W/h·kW
c_p	Specific heat capacity of sea water	J/kg·^{o}C
CTI	Cumulative global irradiance	kJ/m^3
D	Water demand	L/h
d_m	Distillate production of MD m-module	L/h
DP	Total cumulative distillate production	L
d_T	Total distillate production	L/h
F_m	Feed flow rate of MD m-module	L/h
F_m^{Max}	Maximum feed flow rate of MD m-module	L/h
F_m^{Min}	Maximum feed flow rate of MD m-module	L/h
F_T	Feed water source flow rate	L/h
F_T^{Max}	Maximum feed flow rate of feed pump	L/h
F_T^{Min}	Minimum feed flow rate of feed pump	L/h
L_T	Water level of the distillate tank	L
L_T^{Max}	Maximum water level of the distillate tank	L
L_T^{Min}	Minimum water level of the distillate tank	L
L^*	Setopint level of the distillate tank	L
M-STEC	Mean STEC of the MD facility	kWh/m^3
p_i	with $i = 1,\ldots,9$, Polynomial coefficients	–
S_m	Specific thermal energy consumption of MD m-module	kWh/m^3
$T_{cin,m}$	Inlet temperature of the condenser channel of MD m-module	^{o}C
$T_{cout,m}$	Outlet temperature of the condenser channel of MD m-module	^{o}C
$T_{cs,in}$	Inlet temperature at the cold side of the heat exchanger	^{o}C
$T_{cs,out}$	Outlet temperature at the cold side of the heat exchanger	^{o}C

(*continued on next page*)

(*continued*)

Variable	Description	Units
$T_{ein,m}$	Inlet temperature of the evaporator channel of MD *m*-module	ºC
T_{Feed}	Feed water source temperature	ºC
$T_{hs,in}$	Inlet temperature at the hot side of the heat exchanger	ºC
$T_{hs,out}$	Outlet temperature at the hot side of the heat exchanger	ºC
TTEC	Total thermal energy consumption	kWh
V_m	Valve aperture	%
WD	Total cumulative water demand	L
$\alpha^d_{m,j}$	with j = 1…,2, Auxiliary variable 1 for the MILP model	–
$\alpha^T_{m,j}$	with j = 1…2, Auxiliary variable 2 for the MILP model	–
δ_m	Valve position	0–1
ΔT_m	Temperature difference between the inlet of the evaporator channel and the outlet of the condenser channel of the MD *m*-module	ºC
ρ	Density of sea water	kg/m^3

References

[1] A. Deshmukh, C. Boo, V. Karanikola, S. Lin, A.P. Straub, T. Tong, D.M. Warsinger, M. Elimelech, Membrane distillation at the water-energy nexus: limits, opportunities, and challenges, Energy Environ. Sci. 11 (5) (2018) 1177–1196, https://doi.org/10.1039/c8ee00291f.

[2] D. González, J. Amigo, F. Suárez, Membrane distillation: perspectives for sustainable and improved desalination, Renew. Sustain. Energy Rev. 80 (2017) 238–259, https://doi.org/10.1016/j.rser.2017.05.078.

[3] Y. Kim, K. Thu, S.-H. Choi, Solar-assisted multi-stage vacuum membrane distillation system with heat recovery unit, Desalination 367 (2015) 161–171, https://doi.org/10.1016/j.desal.2015.04.003.

[4] G. Zaragoza, A. Ruiz-Aguirre, E. Guillén-Burrieza, Efficiency in the use of solar thermal energy of small membrane desalination systems for decentralized water production, Appl. Energy 130 (2014) 491–499, https://doi.org/10.1016/j.apenergy.2014.02.024.

[5] A. Luo, N. Lior, Critical review of membrane distillation performance criteria, Desalination Water Treat. 57 (43) (2016) 20093–20140, https://doi.org/10.1080/19443994.2016.1152637.

[6] R. Miladi, N. Frikha, A. Kheiri, S. Gabsi, Energetic performance analysis of seawater desalination with a solar membrane distillation, Energy Convers. Manag. 185 (2019) 143–154, https://doi.org/10.1016/j.enconman.2019.02.011.

[7] J.D. Gil, L. Roca, A. Ruiz-Aguirre, G. Zaragoza, M. Berenguel, Optimal operation of a solar membrane distillation pilot plant via nonlinear model predictive control, Comput. Chem. Eng. 109 (2018) 151–165, https://doi.org/10.1016/j.compchemeng.2017.11.012.

[8] I. Janajreh, M.N. Hussain, R. Hashaikeh, R. Ahmed, Thermal efficiency enhancement of the direct contact membrane distillation: conductive layer integration and geometrical undulation, Appl. Energy 227 (2018) 7–17, https://doi.org/10.1016/j.apenergy.2017.10.048.

[9] P. Wang, T.-S. Chung, Recent advances in membrane distillation processes: membrane development, configuration design and application exploring, J. Membr. Sci. 474 (2015) 39–56, https://doi.org/10.1016/j.memsci.2014.09.016.

[10] A. Ruiz-Aguirre, J. Andrés-Mañas, J. Fernández-Sevilla, G. Zaragoza, Experimental characterization and optimization of multi-channel spiral wound air gap membrane distillation modules for seawater desalination, Separ. Purif. Technol. 205 (2018) 212–222, https://doi.org/10.1016/j.seppur.2018.05.044.

[11] M.T. Mito, X. Ma, H. Albuflasa, P.A. Davies, Reverse osmosis (RO) membrane desalination driven by wind and solar photovoltaic (PV) energy: state of the art and challenges for large-scale implementation, Renew. Sustain. Energy Rev. 112 (2019) 669–685, https://doi.org/10.1016/j.rser.2019.06.008.

[12] R. Miladi, N. Frikha, S. Gabsi, Exergy analysis of a solar-powered vacuum membrane distillation unit using two models, Energy 120 (2017) 872–883, https://doi.org/10.1016/j.energy.2016.11.133.

[13] Q. Li, L.-J. Beier, J. Tan, C. Brown, B. Lian, W. Zhong, Y. Wang, C. Ji, P. Dai, T. Li, et al., An integrated, solar-driven membrane distillation system for water purification and energy generation, Appl. Energy 237 (2019) 534–548, https://doi.org/10.1016/j.apenergy.2018.12.069.

[14] A. Shafieian, M. Khiadani, A novel solar-driven direct contact membrane-based water desalination system, Energy Convers. Manag. 199 (2019) 112055, https://doi.org/10.1016/j.enconman.2019.112055.

[15] N. Thomas, M.O. Mavukkandy, S. Loutatidou, H.A. Arafat, Membrane distillation research & implementation: lessons from the past five decades, Separ. Purif. Technol. 189 (2017) 108–127, https://doi.org/10.1016/j.seppur.2017.07.069.

[16] R. Long, X. Lai, Z. Liu, W. Liu, Direct contact membrane distillation system for waste heat recovery: modelling and multi-objective optimization, Energy 148 (2018) 1060–1068, https://doi.org/10.1016/j.energy.2018.02.027.

[17] D. Cheng, W. Gong, N. Li, Response surface modeling and optimization of direct contact membrane distillation for water desalination, Desalination 394 (2016) 108–122, https://doi.org/10.1016/j.desal.2016.04.029.

[18] A. Ruiz-Aguirre, J. Andrés-Mañas, J. Fernández-Sevilla, G. Zaragoza, Modeling and optimization of a commercial permeate gap spiral wound membrane distillation module for seawater desalination, Desalination 419 (2017) 160–168, https://doi.org/10.1016/j.desal.2017.06.019.

[19] J.D. Gil, A. Ruiz-Aguirre, L. Roca, G. Zaragoza, M. Berenguel, Prediction models to analyse the performance of a commercial-scale membrane distillation unit for desalting brines from ro plants, Desalination 445 (2018) 15–28, https://doi.org/10.1016/j.desal.2018.07.022.

[20] H. Deng, X. Yang, R. Tian, J. Hu, B. Zhang, F. Cui, G. Guo, Modeling and optimization of solar thermal-photovoltaic vacuum membrane distillation system by response surface methodology, Sol. Energy 195 (2020) 230–238, https://doi.org/10.1016/j.solener.2019.11.006.

[21] M. Khayet, C. Cojocaru, Artificial neural network modeling and optimization of desalination by air gap membrane distillation, Separ. Purif. Technol. 86 (2012) 171–182, https://doi.org/10.1016/j.seppur.2011.11.001.

[22] W. Cao, Q. Liu, Y. Wang, I.M. Mujtaba, Modeling and simulation of vmd desalination process by ann, Comput. Chem. Eng. 84 (2016) 96–103, https://doi.org/10.1016/j.compchemeng.2015.08.019.

[23] M.-A.A. Hejazi, O.A. Bamaga, M.H. Al-Beirutty, L. Gzara, H. Abulkhair, Effect of intermittent operation on performance of a solar-powered membrane distillation system, Separ. Purif. Technol. 220 (2019) 300–308, https://doi.org/10.1016/j.seppur.2019.03.055.

[24] Y.-H. Chen, Y.-W. Li, H. Chang, Optimal design and control of solar driven air gap membrane distillation desalination systems, Appl. Energy 100 (2012) 193–204, https://doi.org/10.1016/j.apenergy.2012.03.003.

[25] R. Porrazzo, A. Cipollina, M. Galluzzo, G. Micale, A neural network-based optimizing control system for a seawater-desalination solar-powered membrane distillation unit, Comput. Chem. Eng. 54 (2013) 79–96, https://doi.org/10.1016/j.compchemeng.2013.03.015.

[26] J.D. Gil, L. Roca, G. Zaragoza, M. Berenguel, A feedback control system with reference governor for a solar membrane distillation pilot facility, Renew. Energy 120 (2018) 536–549, https://doi.org/10.1016/j.renene.2017.12.107.

[27] A. Ruiz-Aguirre, D.-C. Alarcón-Padilla, G. Zaragoza, Productivity analysis of two spiral-wound membrane distillation prototypes coupled with solar energy, Desalination Water Treat. 55 (10) (2015) 2777–2785, https://doi.org/10.1080/19443994.2014.946711.

[28] D. Cheng, N. Li, J. Zhang, Modeling and multi-objective optimization of vacuum membrane distillation for enhancement of water productivity and thermal efficiency in desalination, Chem. Eng. Res. Des. 132 (2018) 697–713, https://doi.org/10.1016/j.cherd.2018.02.017.

[29] J.D. Gil, J.D. Álvarez, L. Roca, J.A. Sánchez-Molina, M. Berenguel, F. Rodríguez, Optimal thermal energy management of a distributed energy system comprising a solar membrane distillation plant and a greenhouse, Energy Convers. Manag. 198 (2019) 111791, https://doi.org/10.1016/j.enconman.2019.111791.

[30] A.M. Geoffrion, Generalized benders decomposition, J. Optim. Theor. Appl. 10 (4) (1972) 237–260, https://doi.org/10.1007/BF00934810.

[31] E. Camacho, C. Bordons, Model Predictive Control, Springer-Verlag Ltd, London, 2004.

[32] L. Roca, J.A. Sánchez-Molina, F. Rodríguez, J. Bonilla, A. de la Calle, M. Berenguel, Predictive control applied to a solar desalination plant connected to a greenhouse with daily variation of irrigation water demand, Energies 9 (3) (2016) 194, https://doi.org/10.3390/en9030194.

[33] F. Rodríguez, M. Berenguel, J.L. Guzmán, A. Ramírez-Arias, Modeling and Control of Greenhouse Crop Growth, Springer, 2015.

[34] Matlab Release 2018a, the MathWorks, Natick, MA, USA, 2018.

[35] N.V. Sahinidis, BARON V. 2019.7.13: Global Optimization of Mixed-Integer Nonlinear Programs, User's Manual, 2018.

[36] IBM, IBM ILOG CPLEX v. 12.6.1, User's Manual, 2015.